

Article

Experimental Characterization of Oil/Gas Interface Self-Adjustment in CO₂-Assisted Gravity Drainage for Reverse Rhythm Reservoir

Haishui Han ^{1,2}, Xinglong Chen ^{1,2}, Zemin Ji ^{1,2}, Junshi Li ³, Weifeng Lv ^{1,2}, Qun Zhang ^{1,2}, Ming Gao ^{1,2} and Hao Kang ^{4,*}

¹ Research Institute of Petroleum Exploration and Development, PetroChina Company Limited, Beijing 100083, China

² State Key Laboratory of Enhanced Oil Recovery, PetroChina Company Limited, Beijing 100083, China

³ CNPC Advisory Center, PetroChina Company Limited, Beijing 100120, China

⁴ Polytechnic College, Hebei Normal University, Shijiazhuang 050024, China

* Correspondence: haokang@hebtu.edu.cn



Citation: Han, H.; Chen, X.; Ji, Z.; Li, J.; Lv, W.; Zhang, Q.; Gao, M.; Kang, H. Experimental Characterization of Oil/Gas Interface Self-Adjustment in CO₂-Assisted Gravity Drainage for Reverse Rhythm Reservoir. *Energies* **2022**, *15*, 5860. <https://doi.org/10.3390/en15165860>

Academic Editors: Shifeng Zhang, Liangbin Dou, Wenmin Guo, Guoqiang Xing and Yan Zhuang

Received: 3 August 2022

Accepted: 11 August 2022

Published: 12 August 2022

Publisher's Note: MDPI stays neutral with regard to jurisdictional claims in published maps and institutional affiliations.



Copyright: © 2022 by the authors. Licensee MDPI, Basel, Switzerland. This article is an open access article distributed under the terms and conditions of the Creative Commons Attribution (CC BY) license (<https://creativecommons.org/licenses/by/4.0/>).

Abstract: Worldwide practices have proven that gas-assisted gravity drainage can obviously enhance oil recovery, and this technology can be especially effective for reservoirs with a thick formation and large inclination angle. For the successful implementation of this process, a key technology is the stable control of gas–oil interface during gas injection. For a detailed exploration of this technique, a three-stage permeable visual model was designed and manufactured, with permeability decreasing from top to bottom, thus, a reverse rhythm reservoir was effectively modeled. Then the experiment concerning CO₂-assisted gravity drainage was carried out with the adoption of a self-developed micro visual displacement device. This study mainly focused on the micro migration law of gas–oil interface and the development effects of CO₂-assisted gravity drainage. According to the experiments, CO₂ fingering somewhat happens in the same permeable layer from the beginning of gas injection. However, phenomena of “wait” and “gas–oil interface self-adjustment” occur instead of flowing into the next layer when the injected CO₂ reaches the boundary of the next lower permeability layer through the dominant channel. By the “gas–oil interface self-adjustment”, the injected CO₂ first enters into the pores of the relative higher permeability layer to the greatest extent, and thus expands the sweep volume. Furthermore, in the process of CO₂ injection, obvious gas channeling occurs in the low permeability layer directly connected to the outlet, resulting in low sweep efficiency and poor development effect. After connecting the core with lower permeability at the outlet, the development indexes of the model, such as the producing degree of the low permeability layer, the oil recovery before and after gas breakthrough, are significantly improved, and the recovery degrees of the medium permeability layer and the high permeability layer are also improved, and the overall recovery factor is increased by 12.38%. This “gas–oil interface self-adjustment” phenomenon is explained reasonably from the two scales of macroscopic flow resistance and microscopic capillary force. Finally, the enlightenments of the new phenomenon are expounded on the application of gas-assisted gravity drainage on site and the treatment of producers with gas breakthrough in gas injection development.

Keywords: heterogeneous reservoir; gas injection; gas–oil interface self-adjustment; seepage resistance; reverse rhythm

1. Introduction

Compared with immiscible displacement, gas-injected miscible flooding has obvious advantages in improving sweep volume and displacement efficiency. Based on the literature and field experience, Tang et al. pointed out the key issues to be considered and the development trend in the process of CO₂ miscible flooding and emphasized the importance

of miscibility and CO₂ sweep efficiency in the implementation of the technology on site [1]. Based on the investigation of relevant literature worldwide, Li et al. summarized the theoretical research progress of near-miscible gas flooding in reservoirs and pointed out the direction for the study of performance prediction in gas injection development by means of numerical simulation and physical experiments [2]. In view of the lack of uniform screening indexes and screening methods for CO₂ miscible flooding reservoirs, Lei et al. summarized the projects of CO₂ miscible flooding in the world and established a screening model for CO₂ miscible displacement reservoirs by using probability and mathematical statistics methods, fuzzy optimization theory and fuzzy analytic hierarchy process. This method can objectively evaluate the development potential of a reservoir by CO₂ flooding [3]. Liu et al. carried out CO₂ displacement experiments by using different development methods with various parameters in C8 ultra-low permeability reservoirs, and detailed results were obtained concerning the influences towards the recovery degree [4]. Yue et al. conducted caprock breakthrough tests and CO₂ storage experiments with core samples from the Huang-3 block of the Ordos Basin, and the feasibility and influential factors of geological CO₂ sequestration in the Huang-3 area were thoroughly analyzed [5]. At present, gas injection miscible displacement for enhanced recovery has been widely used in the world, especially in North America. According to 2016 data [6,7], the number of gas injection miscible displacement projects was 171, accounting for 89.1% of the total gas injection projects in the world. During the last ten years, gas injection tests have been carried out successively in Daqing, Jilin, Changqing, Talimu, Xinjiang, and other oil fields in China. All of them have obtained some positive effects, but there are still difficulties in their large-scale application. One of the reasons is that it is difficult to realize gas injection miscible flooding in most reservoirs in China due to the nature of the oil [8–12]. However, it has been proved by practice worldwide that gas-assisted gravity drainage (GAGD) can also achieve better EOR results in reservoirs with the characteristics of a thick formation and large dip angle [13–17]. This is of great significance for EOR by gas injection in China's oil reservoir.

GAGD makes full use of the gravity differentiation caused by gas–oil density difference to weaken the gas fingering phenomenon and then expands the gas sweep volume to enhance oil recovery [18,19]. However, in the actual implementation process, the difference in mobility caused by the difference in viscosity between the gas and oil is large, so there is still a wide range of fingering phenomena in the injected gas. Therefore, the stable migration of the gas–oil interface is the key to the successful implementation of GAGD. Actually, many scholars have conducted lots of studies concerning this issue. Based on a large number of statistical samples of successful blocks, Yang et al. introduced a series of dimensionless numbers by drawing on the weight evaluation method and comprehensively using a variety of mathematical statistics theories. Finally, three criteria for the effect analysis of stable gravity flooding by top gas injection are given, and a quantitative evaluation and screening method for top gas injection in mature oilfields with high water cut is established [20]. Liang et al. focused on the key factors affecting the gas-assisted gravity drainage process and the factors that need to be considered when applied to on-site oilfields. According to the study, the stability of gas–oil interface is the key to the success of the gas-assisted gravity drainage process. The key geological and development factors affecting the stability of the gas–oil interface are determined. The study also provides a reliable basis for the selection of the best time for implementing gas-assisted gravity drainage in the oilfield [21]. Concerning the geological conditions and development status of Oubei Block in Jiangsu Oilfield, Zhang et al. established a numerical model of top nitrogen injection gravity flooding and analyzed various factors affecting the development effect of top nitrogen injection gravity flooding in gas-cap reservoirs. On this basis, the development indexes of various schemes are calculated and compared, and the potential of enhanced oil recovery in this block is evaluated. This study can provide a reference for the selection of development modes of similar gas-cap reservoirs [22]. Ren et al. studied the influence of injection rate, reservoir dip angle, crude oil viscosity, and other factors on gravity stable gas injection

to improve oil displacement efficiency through laboratory experiments and analyzed the principle of GAGD to enhance oil recovery. Then, a simplified top gas injection gravity stability discrimination model NGAGI was established theoretically. The effects of reservoir dip angle, permeability, density difference between the displacing fluid and the displaced fluid, oil viscosity, and gas injection rate on the stability of the gravity-stabilized gas-driving front are comprehensively considered, which provides a good foundation for decision-making for on-site oilfield development [23]. However, most of these studies are based on a single-layer reservoir, but there are few reports on the influence of interlayer interface on gas–oil interface migration in reservoirs with different permeability, especially in reverse rhythm reservoirs.

Thick oil reservoirs tend to form large longitudinal permeability differences during the deposition process. We aimed to identify the mechanism of gas–oil interface migration and development effects of GAGD in the reverse rhythm reservoir by designing a three-stage permeability sand filling visual experimental model. A high-speed camera is used to observe the gas–oil interface migration characteristics in the process of GAGD. It is found that the gas–oil interface has an “automatic adjustment” phenomenon at the boundaries of different permeable layers. This new understanding is explained in detail by the seepage theory. Then, the enlightening for GAGD and the treatment for producers with gas channeling is expounded.

2. Materials and Methods

2.1. Model Design and Experimental Materials

Model Design: The purpose of this experiment is to study the law of oil flow by gravity drainage in a reverse rhythm reservoir. In order to determine the permeability and porosity of each single layer, first fill the model with quartz sand of all meshes in sequence, and the permeability of $5455 \times 10^{-3} \mu\text{m}^2$, $3218 \times 10^{-3} \mu\text{m}^2$, $1361 \times 10^{-3} \mu\text{m}^2$ is obtained respectively, with the ratio of quartz sand mesh shown in Table 1. Then the three-layer heterogeneous model is filled with quartz sand with the same mesh ratio. Finally, three-level permeability layers are evenly distributed from top to bottom as a reverse rhythm reservoir, whose permeability is $5455 \times 10^{-3} \mu\text{m}^2$, $3218 \times 10^{-3} \mu\text{m}^2$, $1361 \times 10^{-3} \mu\text{m}^2$, respectively.

Table 1. Quartz sand mesh ratio of reservoirs with different permeability.

Layer NO.	Porosity/%	Perm-Plug Method/ $10^{-3} \mu\text{m}^2$	≤ 60 Mesh/%	60~100 Mesh/%	≥ 100 Mesh/%
1	44.78	5455	63	25	12
2	38.62	3218	47	28	25
3	35.15	1361	30	35	35
Core	23.54	237	–	–	–

The boundary of layers with different permeability are clearly visible. The size of the model is close to the size of the visible window, with a diameter of 10 cm and a thickness of 1.0 cm. The overall seepage characteristics of the model and the migration law of the gas–oil interface can be viewed from a distance with a strong light source. Meanwhile, the microscopic flow of local pore oil can also be observed and recorded through a high-speed camera. The schematic diagram of the model and real products are shown in Figures 1 and 2, respectively.

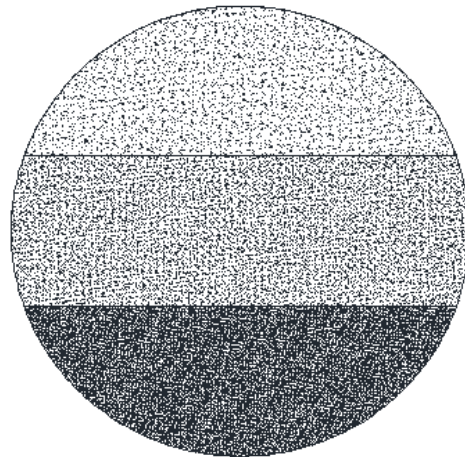


Figure 1. Schematic diagram of reverse rhythm reservoir. Note: The darker the color, the denser the layer.



Figure 2. Visual window diagram.

Experimental Materials: The experimental oil was No.10 aviation kerosene produced by Nanjing Jiangnan Petrochemical Company, and its viscosity under the test environment was 2.42 mPa·s. Due to its color, its movement could be observed clearly in the experiment. Based on the laboratory conditions, CO₂ was used as the injection gas, which was produced by Beijing Zhaoge Gas Technology Company, owning a purity of 99.996%. The petroleum ether (analytically reagent) used for cleaning the experimental device is a product of the Beijing Chemical Plant.

2.2. Experimental Apparatus

The experimental apparatus is the high-temperature and high-pressure microscopic visual oil displacement device independently developed by the Research Institute of Petroleum Exploration and Development, which is mainly composed of four systems: pressure control system, microscopic model system, image acquisition, and analysis system, and auxiliary system. The process diagram is shown in Figure 3.

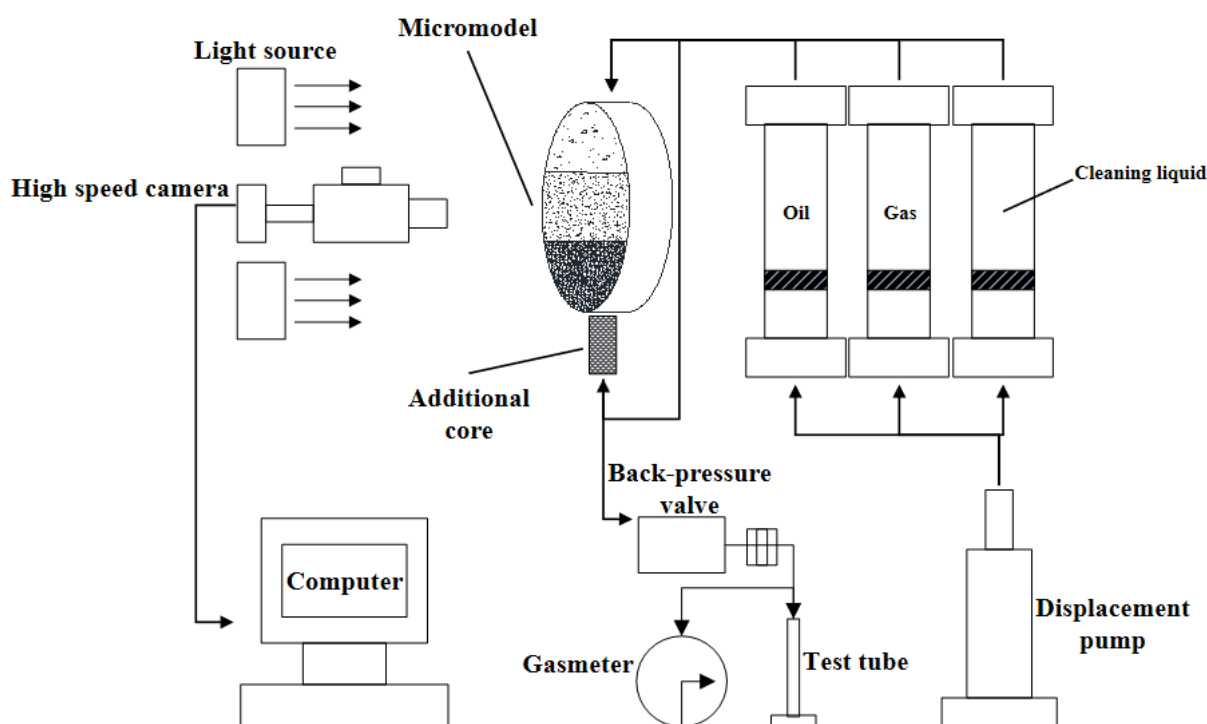


Figure 3. High-temperature and high-pressure microscopic visual oil displacement device.

2.3. Experimental Procedure

The experiments are conducted at room temperature. The outlet is at the bottom of the model and its pressure is set as zero. The inlet is at the top of the model where CO₂ is injected at a constant rate. The specific steps for experiments are as follows:

For the first experiment: (1) Use methanol and petroleum ether to clean the model successively, then sweep the model with nitrogen for vacuum creation. (2) At room temperature, slowly saturate the model with kerosene at a rate of 0.5 mL/min from bottom to top until the injection volume reaches more than twice the pore volume. Turn on the high-speed camera to record in the meantime. (3) Close the inlet and outlet of the model for stabilization of at least 4 h, then CO₂ is slowly injected from the top of the model at the constant rate of 0.1 mL/min. (4) Observe migration of the CO₂–oil interface and the movement of oil in the model. At the same time, record the pressure at the inlet, and record the oil and gas output at the outlet. (5) When the oil is no longer produced, stop the experiment.

For the second experiment: A small section of the real core is connected at the outlet in order to increase flow resistance, whose permeability is $237 \times 10^{-3} \mu\text{m}^2$ and is less than that of the lowest permeability layer in the reverse rhythm reservoir. Then repeat the steps (1)–(5) above and observe the migration of the CO₂–oil interface and the movement of oil in the model. At the same time, record the pressure at the inlet, and record the oil and gas output at the outlet. When the oil is no longer produced, stop the experiment.

3. Results

3.1. Oil Saturation Process

By geometric calculation, the volume of the high, medium, and low permeability layers was obtained as 22.917 cm³, 32.666 cm³, and 22.917 cm³. Combining the data in Table 1, the pore volume of each layer was obtained as 10.262 cm³, 12.616 cm³, and 8.055 cm³, respectively. Therefore, the total pore volume of the model was 30.933 cm³ and the proportions of pore volume in high, medium, and low permeability layers were 33.17%, 40.79%, and 26.04%, respectively. According to the experiment design, the oil saturation process is carried out from the bottom to the top. The interface migration process

is shown in Figure 4. The red dotted line shows the boundaries of high, medium, and low permeability layers, and the yellow dotted line is the saturated oil interface. High, medium, and low permeability layers have different light transmittances. The high permeability layers have strong light transmittance and the low permeability layers have weak light transmittance. In order to clearly observe the saturated oil interface, the backlight intensity should be adjusted in time during the oil saturation process. As shown in Figure 4, the saturated oil interface migrated evenly and steadily from the bottom to the top with basically no fingering phenomenon, and the final oil saturation was relatively sufficient. As shown in Figure 5, the relationship between the rising height of the saturated oil interface and the amount of injected oil was established. Since the model was circular, the rising height of the liquid level and the amount of oil injected were not linear. Kerosene was evenly saturated along the low permeability layer, medium permeability layer, and high permeability layer in turn. This is because, on the one hand, the speed of saturated oil was slow, which gives full play to the gravity properties of kerosene. On the other hand, there was only one fluid, with no mobility difference between different fluids in the model. Table 2 shows the final saturated oil profile for each layer. The model actually contained only a few dead pores because it was a sand-filled model. The kerosene was sufficiently saturated and the total oil saturation reached about 95.37%.

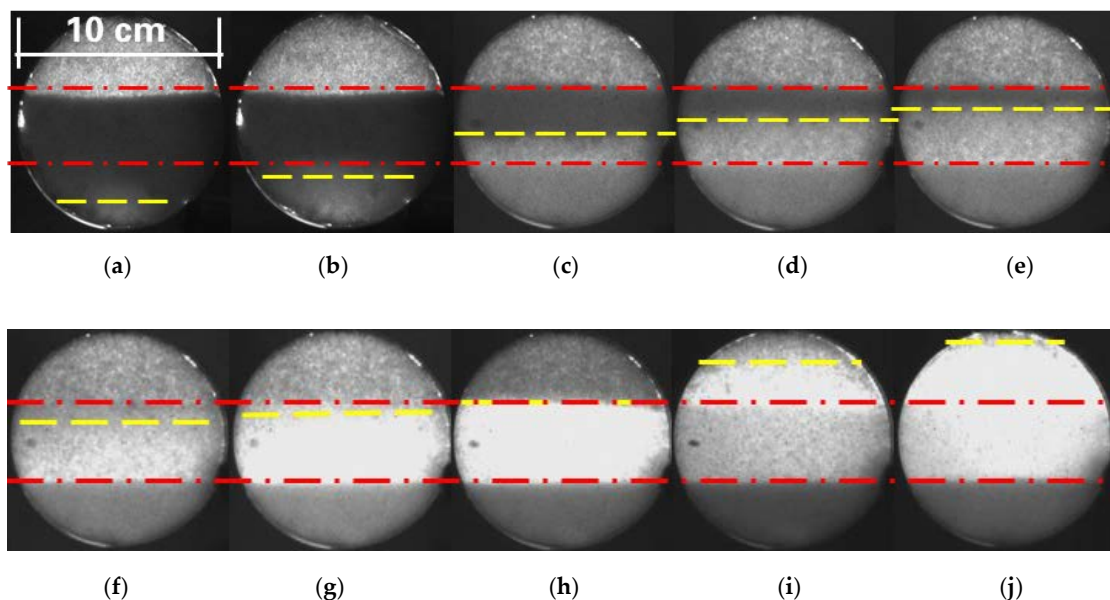


Figure 4. Interface migration of oil saturation process. (a) 0.21 HCPV, (b) 0.42 HCPV, (c) 0.62 HCPV, (d) 0.80 HCPV, (e) 1.03 HCPV, (f) 1.27 HCPV, (g) 1.42 HCPV, (h) 1.63 HCPV, (i) 1.83 HCPV, (j) 2.23 HCPV. Note: The yellow dotted line is the saturated oil interface; the red dotted line is the interface between layers with different permeability.

3.2. CO₂-Assisted Gravity Drainage

In order to fully reflect the gravity differentiation between CO₂ and oil, CO₂ was injected from the high permeability layer at the top and the gas injection rate was set as small as possible (0.1 mL/min). The high-speed camera recorded the gas–oil interface migration process at different moments, as shown in Figure 6. As we can see in the Figure, CO₂ is darker than oil in color. Then analyzing the image carefully, the gas–oil interface migration laws can be summarized as follow.

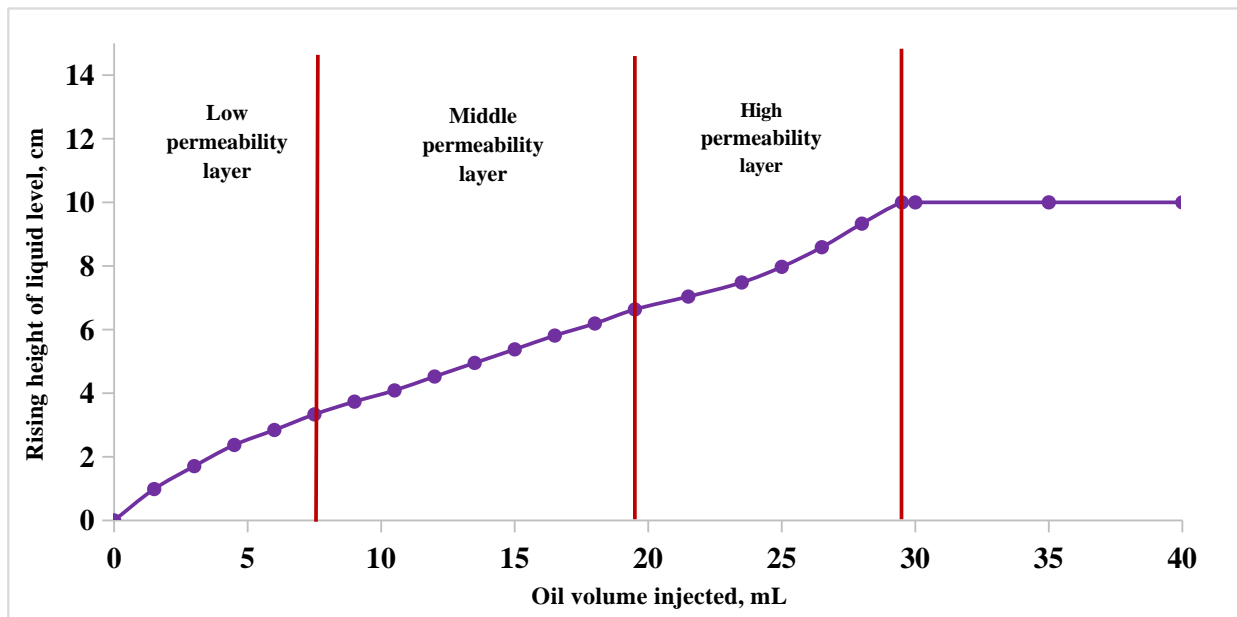


Figure 5. Relation between the rising height of liquid level and the amount of injected oil in the process of oil saturation.

Table 2. Saturated oil status in different permeability layers.

Layer Position	Saturated Oil Volume/mL	Saturation Ratio/%	Pore Volume/mL	Single Layer Saturation/%
High permeability layer	10.00	33.90	10.26	97.45
Medium permeability layer	12.00	40.68	12.62	95.12
Low permeability layer	7.50	25.42	8.06	93.11
Summary	29.50	100.00	30.93	95.37

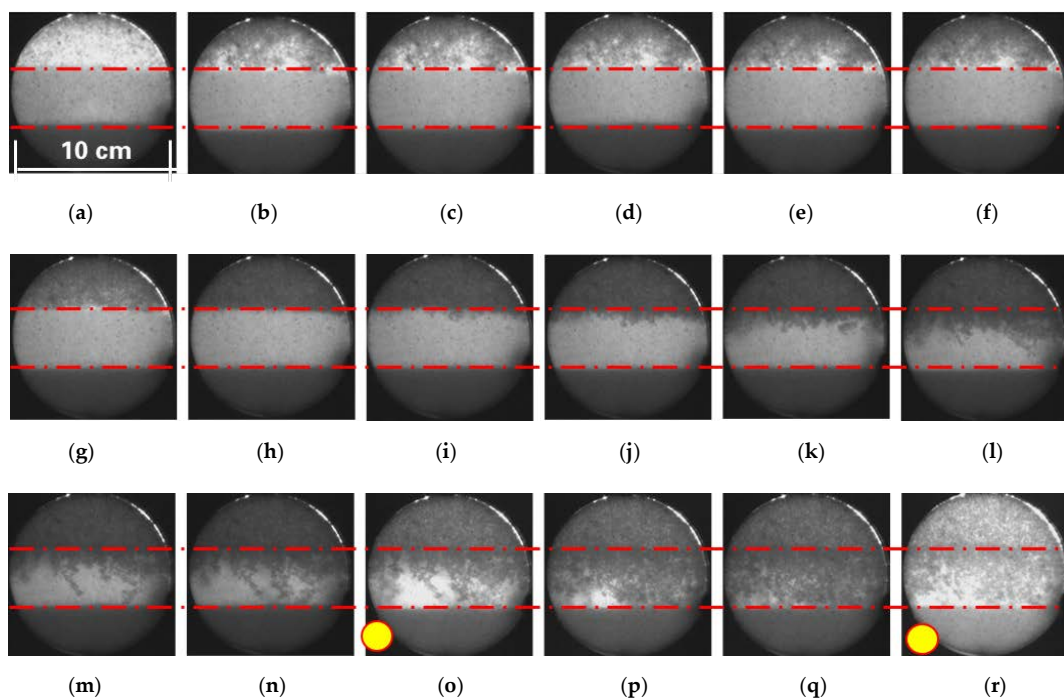


Figure 6. Cont.

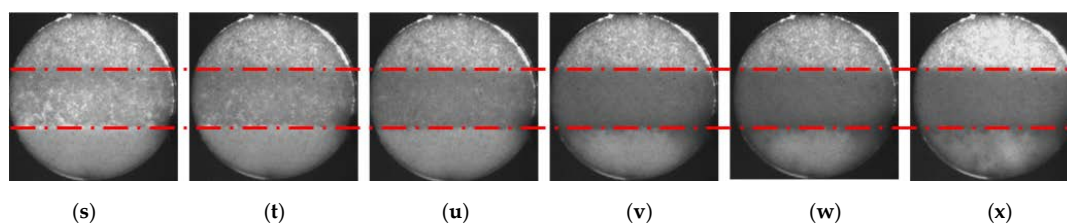


Figure 6. Gas–oil interface migration during CO₂-assisted gravity drainage. (a) 0.01 HCPV, (b) 0.04 HCPV, (c) 0.07 HCPV, (d) 0.10 HCPV, (e) 0.13 HCPV, (f) 0.17 HCPV, (g) 0.20 HCPV, (h) 0.23 HCPV, (i) 0.26 HCPV, (j) 0.29 HCPV, (k) 0.32 HCPV, (l) 0.35 HCPV, (m) 0.38 HCPV, (n) 0.41 HCPV, (o) 0.44 HCPV, (p) 0.47 HCPV, (q) 0.50 HCPV, (r) 0.53 HCPV, (s) 0.55 HCPV, (t) 0.57 HCPV, (u) 0.59 HCPV, (v) 0.68 HCPV, (w) 1.25 HCPV, (x) 1.45 HCPV. Note: The red dotted line is the interface between layers with different permeability; the yellow circle is the moment of light brightening.

(1) Free seepage stage in each flow direction of high permeability layer

As shown in images (a) to (d), although there is a gravity difference (density difference) between CO₂ and oil and the injection rate of CO₂ is small, the gas–oil interface was not obvious after CO₂ entered the high permeability layer and oil was not uniformly pushed downward by the CO₂. CO₂ migrated downward at relatively different speeds in all directions, and the time to reach the boundary between the high and the medium permeability layer was also different, where the general direction of the streamline was the same but the distribution was disordered. At the time of image (b), CO₂ reached the boundary between two layers through the channel with good permeability. At the time of image (d), CO₂ had already arrived the boundary through most of the flow channels.

(2) Self-adjustment stage in high permeability layer

As shown in images (e) to (h), when CO₂ reached the boundary between the high and medium permeability layers along a certain channel, it did not continue to migrate to the lower permeability layer for oil displacement, but a “wait” occurred for not-arrived CO₂ in other channels, until CO₂ almost filled the seepage space of the entire high permeability layer. This made the CO₂ sweep volume maximum in the high permeability layer.

(3) Restart stage in medium permeability layer

From the moment (i), CO₂ restarted to move down again to displace the oil in the medium permeability layer after the interface between the high and medium permeability layers were fully filled with CO₂. As shown in images (i) to (n), the gas preferentially traveled along the relatively high-permeability channel to reach the medium and low permeability interface. In the figures, the gas breakthrough was obvious and the gravity differentiation between CO₂ and oil was difficult to manifest.

(4) Self-adjustment stage in medium permeability layer

The lower the permeability of the layers, the worse the light transmission performance. In order to clearly observe the migration rule of the gas–oil interface, the light was brightened twice at the moment (o) and (r). Images (o)~(u) show that the process was similar to the self-adjustment of the high-permeability layer after the gas reached the boundary of the medium and low permeability layers. The difference was that the pore volume of the medium permeability layer was larger than that of the high permeability layer, and the self-adjustment duration was longer than that in the high permeability layer.

(5) Sprint stage in low permeability layer

Similarly, after the interface between the medium and low permeability layers were generally fully filled with CO₂, CO₂ began to restart and move down to displace the oil at the low permeability layer from the time (v). From images (v) to (x), CO₂ at this stage preferentially reached the bottom quickly along a few dominant channels. After reaching

the exit, it did not “wait” for the low-permeability layer to be filled with CO₂, but it directly flowed out of the model and thus formed fluid channeling. Under this circumstance, the gas–oil gravity differentiation effect was difficult to reflect and the sweep efficiency of CO₂ was relatively poor in the low permeability layer.

The relation between the production degree, gas–oil ratio and injection volume in the process of CO₂ injection is shown in Figure 7, and the production degree of each rhythm layer is shown in Table 3. When the injection volume was 0.23 HCPV, the injected CO₂ was self-adjusted in the high permeability layer and the recovery degree was 20.21%. Then the injected CO₂ permeated and displaced the oil in the medium permeability layer. When the injection volume was 0.59 HCPV, the injected CO₂ was self-adjusted in the medium permeability layer, and the total recovery degree was 46.22%. Later, the injected CO₂ migrates into the low permeability layer to displace the oil. When the injection volume was 0.68 HCPV, there was a gas breakthrough happening at the bottom of the model and the recovery degree was 49.97%. After that, the gas–oil ratio increased rapidly and the oil production decreased. When the injection volume was 1.45 HCPV, the model basically could not produce oil anymore and the ultimate recovery efficiency was 55.13%.

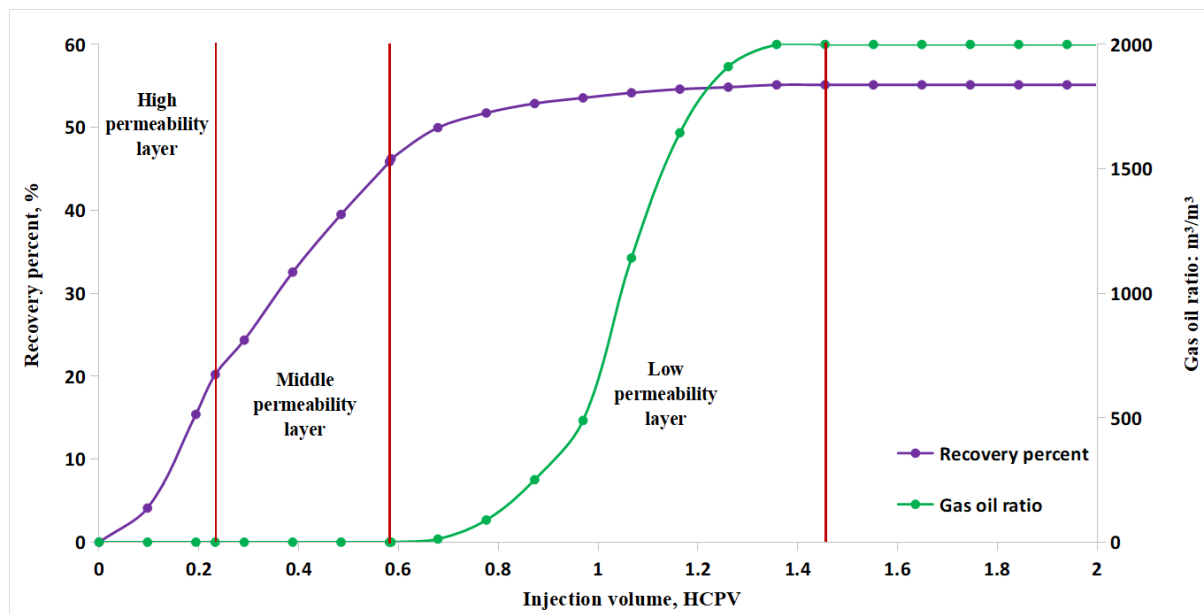


Figure 7. Relation between the recovery percent, gas–oil ratio and injection volume in the CO₂ injection process.

Table 3. Recovery percent of each rhythm layer.

Layer/Stage	HCPV	Total Recovery Degree, %	Stage Recovery Degree, %
High permeability layer	0.23	20.21	20.21
Medium permeability layer	0.59	46.22	26.01
Low permeability layer	1.45	55.13	8.91
Production before gas breakthrough	0.68	49.97	49.97
Production after gas breakthrough	1.45	55.13	5.16

During the drainage process before and after the gas breakthrough, the oil production degree was 49.97% and 5.16%, respectively. The oil production contribution of the three layers with high, medium, and low permeability was 20.21%, 26.01%, and 8.91%, respectively. High permeability and medium permeability layers contributed 83.84% of the model’s total recovery efficiency and only 16.16% was contributed by the low permeability layer. There was still a large amount of remaining oil in the low permeability layer that had not been

produced. If this portion of oil can be produced effectively, the total recovery efficiency of the reverse rhythm reservoir will be greatly improved.

3.3. CO₂ Drainage after Increasing Flow Resistance at Output

Based on a previous study on the interface migration law of CO₂ assisted gravity drainage (Figure 6), it was found that when CO₂ reached the boundaries between rhythmic layers, there was a self-adjustment process between the high and medium permeability layers: CO₂ migrated down only after it occupied the pore spaces as much as possible within the same layer. However, there was also an exception, in that the injection of CO₂ in the low permeability layer lacked a self-adjustment process, and CO₂ quickly reached the outlet to form a gas breakthrough, which resulted in a small recovery efficiency in the low permeability layer.

Therefore, another experiment was designed to keep all the other conditions the same, except that a short core with a permeability of $237 \times 10^{-3} \mu\text{m}^2$ was added at the outlet, which was of much less permeability than that of the low permeability layer. The main objective of this experiment was to study whether this new drainage process could improve the development effects in the low permeability layer.

The high-speed camera was also used to record the migration process of the gas–oil interface at different times, as shown in Figure 8. Through careful analysis of the images, it was found that the gas–oil interface migration went through the following stages.

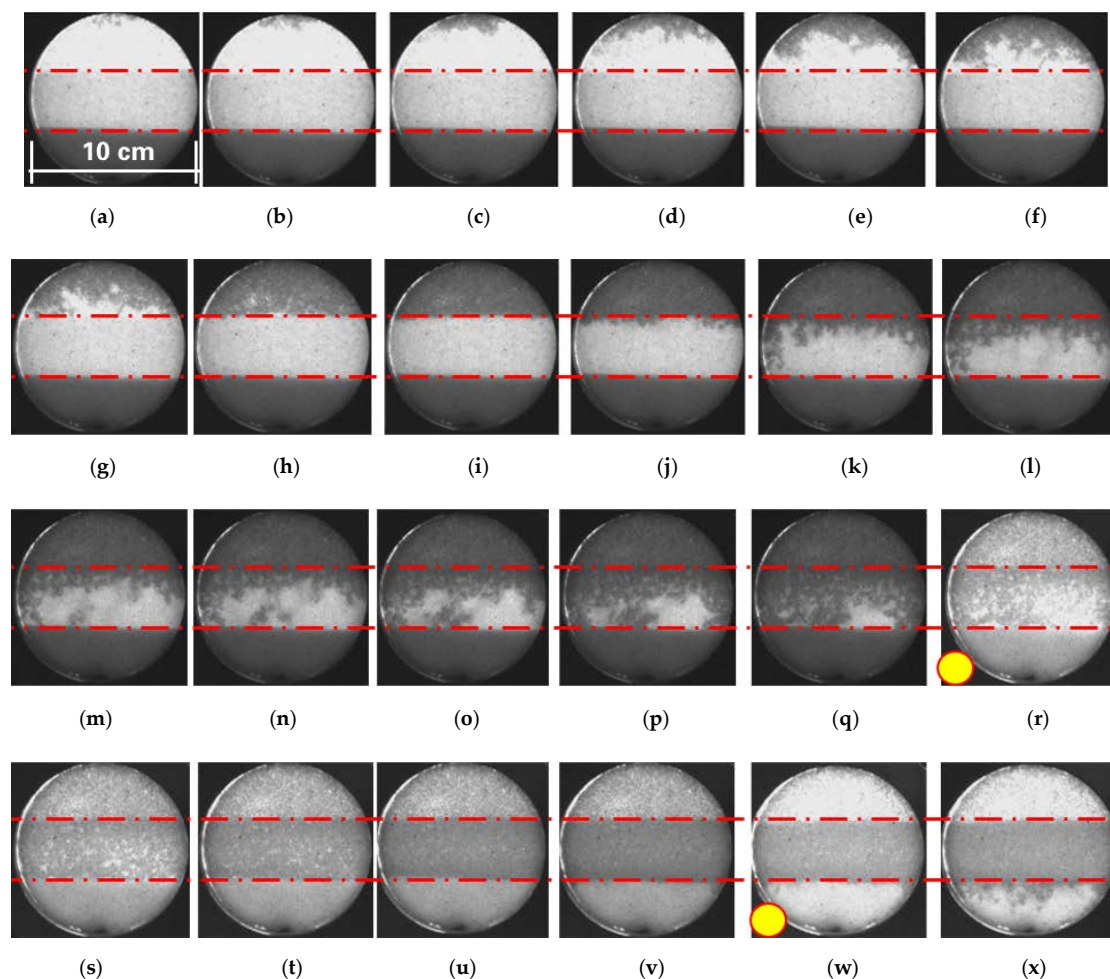


Figure 8. Cont.

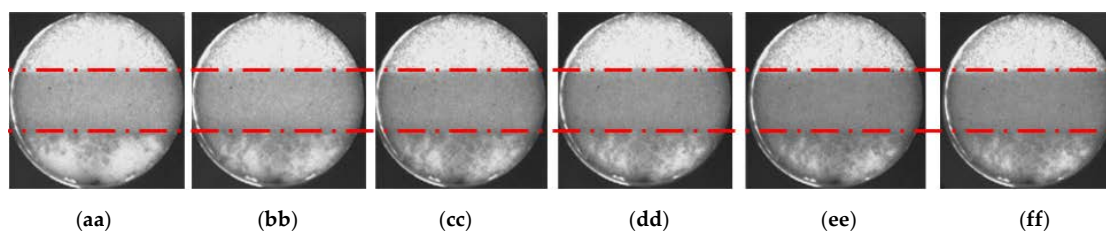


Figure 8. Gas–oil interface migration during CO₂-assisted gravity drainage after increasing resistance. (a) 0.01 HCPV, (b) 0.03 HCPV, (c) 0.05 HCPV, (d) 0.07 HCPV, (e) 0.09 HCPV, (f) 0.11 HCPV, (g) 0.15 HCPV, (h) 0.20 HCPV, (i) 0.24 HCPV, (j) 0.27 HCPV, (k) 0.30 HCPV, (l) 0.33 HCPV, (m) 0.36 HCPV, (n) 0.39 HCPV, (o) 0.42 HCPV, (p) 0.45 HCPV, (q) 0.48 HCPV, (r) 0.51 HCPV, (s) 0.54 HCPV, (t) 0.56 HCPV, (u) 0.58 HCPV, (v) 0.60 HCPV, (w) 0.63 HCPV, (x) 0.66 HCPV, (aa) 0.69 HCPV, (bb) 0.72 HCPV, (cc) 0.75 HCPV, (dd) 0.78 HCPV, (ee) 1.14 HCPV, (ff) 1.55 HCPV. Note: The red dotted line is the interface between layers with different permeability; the yellow circle is the moment of light brightening.

- (1) Free seepage stage in each flow direction of high permeability layer, which corresponds to images (a)~(f) in Figure 8. The gas–oil interface migration rule is consistent with images (a)~(d) in Figure 6.
- (2) Self-adjustment stage in high permeability layer, which corresponds to images (g)~(i) in Figure 8. The gas–oil interface migration rule is consistent with images (e)~(h) in Figure 6.
- (3) Restart stage in medium permeability layer, which corresponds to images (j)~(o) in Figure 8. The gas–oil interface migration rule is consistent with images (i)~(n) in Figure 6.
- (4) Self-adjustment stage in medium permeability layer, which corresponds to images (p)~(v) in Figure 8. The gas–oil interface migration rule is consistent with images (o)~(u) in Figure 6, and the light is brightened at the time of image (r) in Figure 8.
- (5) Restart stage in low permeability layer, which corresponds to images (w)~(aa) in Figure 8. The light is brightened at the time of image (w) in Figure 8 and injected CO₂ started to enter the position of bottom exit along the dominant channel.
- (6) Self-adjustment continuous oil recovery stage in low permeability layer, which corresponds to images (bb)~(dd) in Figure 8. After CO₂ reached the bottom outlet, a similar process happened with that in the high and medium permeability layers. In this stage, self-adjustment of CO₂/oil interface happened and oil is produced continuously until the maximum CO₂ sweep efficiency is realized in the low permeability layer under this condition.
- (7) Continuous oil recovery stage after CO₂ breakthrough, which corresponds to images (dd)~(ff) in Figure 8. In this stage, CO₂ could still displace some oil after breakthrough.

3.4. Comparison of Development Index after Increasing Resistance

After increasing the flow resistance with the supplementary core, the relationship in GAGD between the recovery degree, gas–oil ratio, and injection volume is shown in Figure 9, and the recovery degree of each rhythm layer is shown in Table 4. When the injection volume was 0.24 HCPV, the injected CO₂ was self-adjusted in the high permeability layer and the recovery degree was 21.79%. Then the injected CO₂ penetrated into the medium permeability layer to displace the oil. When the injection volume was 0.60 HCPV, the injected CO₂ was self-adjusted in the medium permeability layer and the total recovery degree was 48.72%. Later, CO₂ continuously flowed into the low permeability layer for oil displacement. When the injection volume was 0.78 HCPV, there started to be CO₂ breakthrough at the bottom of the model and the recovery degree was 59.81%—after that, the gas–oil ratio increased rapidly and the oil production decreased. When the injection volume was 1.55 HCPV, the model basically could not produce oil anymore and the ultimate recovery efficiency was 67.51%.

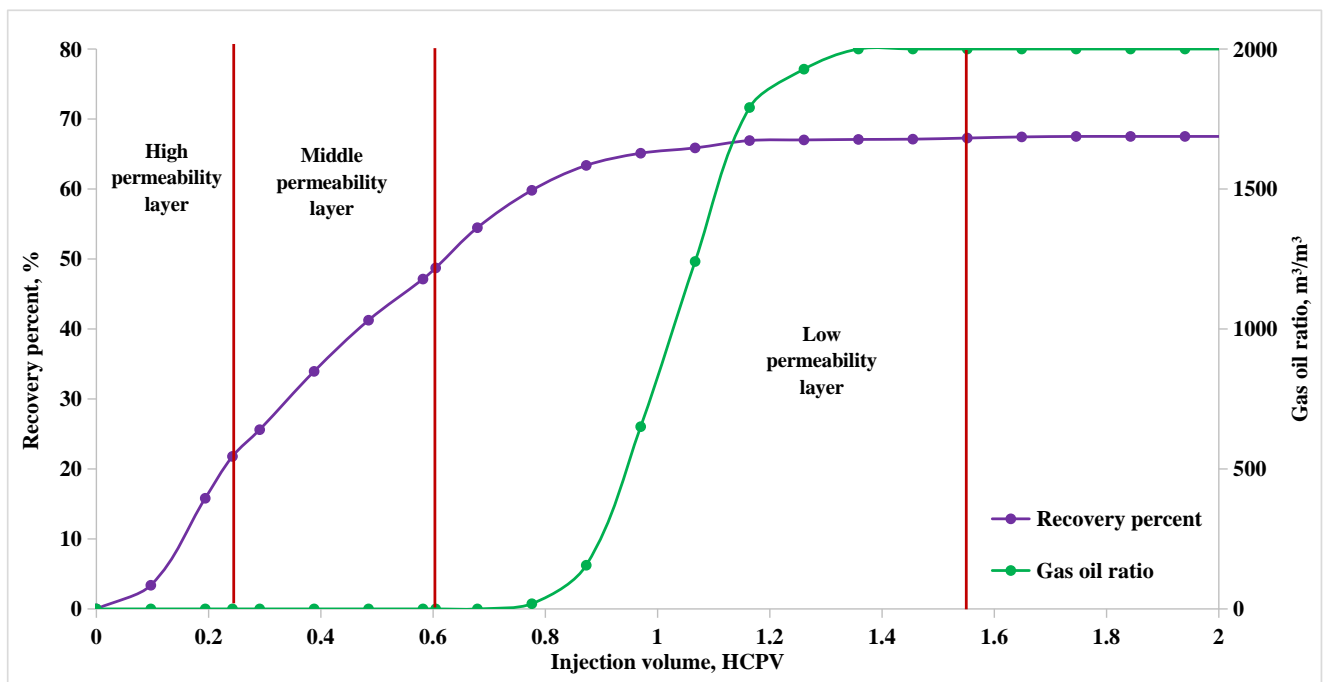


Figure 9. Relation between the recovery degree, gas–oil ratio, and injection quantity in the top gas injection process after increasing resistance.

Table 4. The recovery degree of each rhythm layer after flow resistance is added.

Layer/Stage	HCPV	Total Recovery Degree, %	Stage Recovery Degree, %
High permeability layer	0.24	21.79	21.79
Medium permeability layer	0.60	48.72	26.93
Low permeability layer	1.55	67.51	18.79
Production before gas breakthrough	0.78	59.81	59.81
Production after gas breakthrough	1.55	67.51	7.70

For the drainage process before and after gas breakthrough, the oil recovery degree was 59.81% and 7.70%, respectively. The oil production contribution of the three layers with high, medium, and low permeability was 21.79%, 26.93%, and 18.79%, respectively. Concerning the recovery degree of the whole model, there was 72.17% contributed by high and medium permeability layers and 27.83% contributed by the low permeability layer.

Based on a comprehensive analysis of the data, it can be found that increasing the core resistance at the model outlet has a significant improvement in the development effect of GAGD. The specific performance is as follows:

(1) The total recovery efficiency of the model has increased from 55.13% to 67.51%, an increase of 12.38%. (2) The recovery of oil in the low permeability layer has greatly increased from 8.91% to 18.79%, which is an increase of 9.88%. (3) The recovery of oil in the medium and high permeability layers has also been increased and the recovery degree has been increased by 0.92% and 1.58%, respectively. (4) The period of oil recovery without gas breakthrough has been extended and the recovery degree has increased from 49.97% to 59.81%, which is increased by 9.84%. (5) The amount of oil recovery after gas breakthrough has been improved and the corresponding recovery degree has been increased from 5.16% to 7.70%.

4. Discussion

4.1. Theoretic Analysis

According to the classical seepage theory (Darcy's law), as shown in Formula (1), the fluid seepage velocity in the reservoir depends on the fluidity and pressure gradient. In the process of gas displacement, gas has a lower viscosity, higher fluidity, and higher seepage velocity than oil. Gas fingering is very likely to occur, which will lead to a premature gas breakthrough, low sweep efficiency, and low oil recovery. This displacement effect is fully verified in the first group of experiments. There is strong fingering happened in the initial stage of gas permeating in each rhythm layer, which is more obvious when gas enters into the lower permeability layers. The sweep efficiency and recovery degree in lower permeability layers are very low.

$$v = \frac{K}{\mu} \frac{dp}{dL} = \lambda \cdot \text{grad}(p) \quad (1)$$

However, in addition to the above-mentioned conventional phenomena and effects, completely different phenomena is also shown concerning the gas–oil interface migration during this designed experiment. When CO₂ along a certain channel reaches the boundary of layers with different permeability, it does not continue to flow downward for oil displacement, but a “wait” occurs for the following CO₂ in other channels in the same layer, and an “interface self-adjustment” process happens to expand the sweep volume in this layer until injected CO₂ fills the pore space as much as possible. Only after this process does the injected CO₂ “start” to enter into the next layer downward with relatively lower permeability.

In fact, the above-mentioned unconventional phenomenon that occurred during the experiment is essentially caused by changes in seepage resistance (flow resistance), which can be analyzed and explained from the following two perspectives.

(1) Perspective of macroscopic flow

In the same permeable layer, fingering could easily occur in the CO₂ displacement process due to the difference in CO₂ and oil mobility ratios and heterogeneity in the layer. When encountering a lower permeability layer, the flow resistance of CO₂ will suddenly increase. If the increase in flow resistance caused by the heterogeneity between the layers is greater than that within the layer, CO₂ will preferentially flow into the other channels in the layer. Thus the phenomenon of “wait” and “interface self-adjustment” occurs during the experiment. After the flow resistance within the layer become greater than that between layers, CO₂ “starts” to enter into the next layer with relatively lower permeability.

(2) Perspective of microscopic flow

In the same permeable layer, the radius distribution of the pore throat is relatively concentrated and the pore throat in the high permeability layer has a large radius and small flow resistance, while the pore throat in the low permeability layer has an opposite phenomenon that the radius is relatively small and flow resistance is large.

When the gas/oil interface of CO₂ displacement encounters a lower permeability layer during the flow process, the radius of the gas flow channel becomes smaller and the capillary force acting as the flow resistance suddenly increases. Under this condition, the “gas resistance effect” occurs, also known as the Jamin effect which is demonstrated in Figure 10. The bubbles must be deformed to enter into the smaller pore/throat of the lower permeability layer. If the additional resistance generated during the deformation process is greater than the resistance for entering into the pore/throat in the same layer, CO₂ will preferentially enter into the other pore/throat in the same layer for oil displacement. Therefore, the phenomena “wait” and “interface self-adjustment” will occur when the size of the remaining unswept pore/throat in the co-permeable layer is equivalent to the pore/throat size in the relatively lower permeability layer, the gas “starts” to enter into the lower permeability layer for oil displacement.

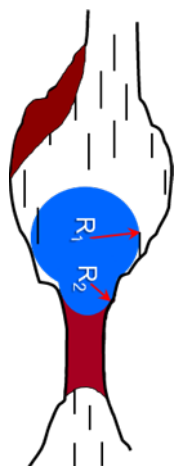


Figure 10. Schematic diagram of Jamin effect in gas displacement.

According to the comparative experiment, the interpretation of these two respects has been further verified. If the low-permeability layer is directly connected to the outlet (as that in the first experiment), the phenomenon of “wait” and “interface self-adjustment” does not occur. However, if a section of the lower permeability core is connected between the low permeability layer and the outlet of the model (as that in the second experiment), the phenomenon of “wait” and “interface self-adjustment” also occurs in the low-permeability layer.

4.2. Enlightenment in Oil Field Development

At present, two main problems in terms of oil field development by GAGD are as follows: (1) How to control the stable migration of the gas–oil interface to maximize the sweep volume of the injected gas. (2) How to ensure continued production to improve recovery efficiency after gas breakthrough happens in the production well.

The key to the successful implementation of GAGD is to effectively ensure that the gas–oil interface can migrate downward steadily. Actually, the reservoir can generally be divided into three types: positive rhythm reservoir, relatively homogeneous reservoir, and reverse rhythm reservoir. According to the results in this paper, there are “wait” and “interface self-adjustment” phenomena when the injected gas reaches the low permeability layer from the high permeability layer. It can be inferred that the gas–oil interface migration in the reverse rhythm reservoir is relatively more stable and the sweep efficiency is relatively larger. The effects in a homogeneous reservoir will be relatively poorer than reverse rhythm reservoir and the effects in a positive rhythm reservoir will be the worse. The gas–oil interface stability can be adjusted to a certain extent through the optimization of the gas injection rate. The order of the optimal injection rate of the three types of reservoirs should be reverse rhythm reservoir, homogeneous reservoir, and positive rhythm reservoir. Therefore, a reverse rhythm reservoir should be given priority for the successful application of GAGD. For GAGD in the positive rhythm reservoir, the injector–producer deployment and injection–production parameters should be strictly controlled. In addition, if there are small-scale interlayers in the reservoir, they can usually play a positive role in the interface control and thus should be fully utilized.

During the horizontal displacement of injected gas, it is easy for fingering to occur along the dominant channel, resulting in gas channeling in some production wells. Oil production decreases rapidly after the gas breakthrough happens, making it difficult to continue production, and there is no effective control method at present. According to the findings and principles of these experiments, if appropriate flow resistance can be added in the bottom of gas-channeling producers, the gas will then penetrate into the surrounding non-swept pores by “self-adjustment” mechanism, which will effectively improve the gas channeling in producers.

5. Conclusions

In the experiment of GAGD in the reverse rhythm reservoir, CO₂ has an obvious fingering phenomenon in the same permeable layer. After CO₂ reaches the boundary of the relatively lower permeability layer along the dominant channel, instead of continuing to flow downward for oil displacement, the phenomenon of “wait” and “gas–oil interface self-adjustment” occurs until the seepage space of the relatively higher permeability layer is filled to the maximum extent. Therefore, the sweep volume of CO₂ in the relatively higher permeability layer is expanded through this “gas–oil interface self-adjustment” mechanism. In the process of GAGD in the reverse rhythm reservoir, gas channeling will occur obviously and the sweep efficiency will be low if the low permeability layer at the bottom is directly connected to the outlet. After connecting the lower permeability core at the end of the outlet, the oil recovery of the low permeability layer and the recovery degree before and after the gas-breakthrough period are all significantly improved. The recovery degree in the medium and high permeability layers has obtained effective improvement and the overall recovery efficiency of CO₂-assisted gravity drainage is increased by 12.38%.

The new laws discovered in the study are explained reasonably from the two perspectives of both macroscopic flow and microscopic flow. The enlightenment for GAGD application and treatment for gas-channeling producers is comprehensively expounded. However, due to the limitations of the study, although there are great advantages of gas injection miscible flooding compared with immiscible flooding, miscible flooding is not seriously considered in these experiments. In future experiments followed, miscible flooding will be designed and tested to find out more insights concerning GAGD.

Author Contributions: Conceptualization, H.H., X.C., Z.J. and H.K.; methodology, H.H., X.C., Z.J. and H.K.; software, X.C., Z.J. and J.L.; formal analysis, H.H., X.C. and H.K.; investigation, M.G.; resources, M.G.; writing—original draft preparation, H.H. and H.K.; writing—review and editing, H.K.; supervision, Q.Z. and W.L.; project administration, Q.Z., M.G. and W.L.; funding acquisition, Q.Z. and W.L. All authors have read and agreed to the published version of the manuscript.

Funding: This research was funded by the major science and technology projects of the Petrochina Company Limited, grant number 2021ZZ01 and by the State Key Laboratory of Enhanced Oil Recovery, Petrochina Company Limited, grant number 2022-KFKT-29.

Conflicts of Interest: The authors declare no conflict of interest.

References

1. Tang, Y.; Yin, P.; Wang, Y.; Sun, B.; Hou, D. Feasibility Assessment of the CO₂ Miscible Flooding Process. *J. Southwest Pet. Univ.* **2014**, *36*, 133–138. [[CrossRef](#)]
2. Li, J.; Li, X.; Liu, B.; Jiang, T. Advancement of Oilfield Development Theory of Near-miscible Gas Flooding. *Nat. Gas Ind.* **2006**, *26*, 108–110. [[CrossRef](#)]
3. Lei, H.; Gong, C.; Guan, B. New screening method for reservoir by CO₂ injection miscible flooding. *J. China Univ. Pet.* **2008**, *32*, 72–76. [[CrossRef](#)]
4. Liu, F.; Yue, P.; Wang, Q.; Yu, G.; Zhou, J.; Wang, X.; Fang, Q.; Li, X. Experimental Study of Oil Displacement and Gas Channeling during CO₂ Flooding in Ultra—Low Permeability Oil Reservoir. *Energies* **2022**, *15*, 5119. [[CrossRef](#)]
5. Yue, P.; Zhang, R.; Sheng, J.J.; Yu, G.; Liu, F. Study on the Influential Factors of CO₂ Storage in Low Permeability Reservoir. *Energies* **2022**, *15*, 344. [[CrossRef](#)]
6. Koottungal, L. 2014 worldwide EOR survey. *Oil Gas J.* **2014**, *112*, 79–91.
7. Sandra, R.; Dharod, D. Approach screens reservoir candidates for EOR. *Oil Gas J.* **2016**, *114*, 48–51.
8. Qin, J.; Han, H.; Liu, X. The application and enlightenment of Carbon Dioxide flooding in United State. *Pet. Explor. Dev.* **2015**, *42*, 209–216. [[CrossRef](#)]
9. Wang, G.; Zheng, X.; Zhang, Y.; Lv, W.; Wang, F.; Yin, L. A new screening method of low permeability reservoirs suitable for CO₂ flooding. *Pet. Explor. Dev.* **2015**, *42*, 358–363. [[CrossRef](#)]
10. Hu, Y.; Hao, M.; Chen, G.; Sun, R.; Li, S. Technologies and practice of CO₂ flooding and sequestration in China. *Pet. Explor. Dev.* **2019**, *46*, 716–727. [[CrossRef](#)]
11. Yang, H.; Lin, L.; Chen, L.; Yu, Y.; Li, D.; Tian, J.; Zhou, W.; He, J. Characteristics of Mineralogy, Lithofacies of Fine-Grained Sediments and Their Relationship with Sedimentary Environment: Example from the Upper Permian Longtan Formation in the Sichuan Basin. *Energies* **2021**, *14*, 3662. [[CrossRef](#)]

12. Xu, L.; Li, H. A Modified Multiple-Mixing-Cell Method with Sub-Cells for MMP Determinations. *Energies* **2021**, *14*, 7846. [[CrossRef](#)]
13. Jiang, Y.; Yang, J.; Chen, D. Research and application of gravity drainage in steam flooding: an example from the high-dip angle area of Qi-40 block in Liaohe oilfield. *Oil Gas Geol.* **2012**, *33*, 938–943.
14. Tian, H. Experimental Study on Waterflooding Law of High Dip Reservoir. *Contemp. Chem. Ind.* **2021**, *50*, 1632–1635. [[CrossRef](#)]
15. Qiao, S.; Geng, W.; Zhang, X.; Tan, J. Key Technology Policy of Natural Gas Gravity Drive-Take Northern Liuzan Block of Nanpu Sag for Example. *Oil Forum* **2022**, *41*, 32–38. [[CrossRef](#)]
16. Feng, K.; Mu, L.; Yan, Y.; Wu, Z.; Li, Q.; Zhang, Y. Numerical simulation of the enhanced oil recovery by gas-assisted gravity drainage (GAGD). *Pet. Geol. Oilfield Dev. Daqing* **2020**, *39*, 77–86. [[CrossRef](#)]
17. Yang, X.; Wang, R.; Deng, X.; Li, S.; Zhang, H.; Yao, C. Theoretical exploration of water injection gravity flooding oil in ultra-deep fault-controlled fractured-cavity carbonate reservoirs. *Pet. Explor. Dev.* **2022**, *49*, 116–124. [[CrossRef](#)]
18. Saikia, B.D.; Rao, D.N. A Single-Well Gas-Assisted Gravity Drainage Enhanced Oil Recovery Process for U.S. Deepwater Gulf of Mexico Operations. *Energies* **2021**, *14*, 1743. [[CrossRef](#)]
19. Grattoni, C.A.; Jing, X.D.; Dawe, R.A. Dimensionless groups for three-phase gravity drainage flow in porous media. *J. Pet. Sci. Eng.* **2001**, *29*, 53–65. [[CrossRef](#)]
20. Yang, C.; Li, Y.; Han, J.; Xu, X. Quantitative evaluation and screening method for gas assisted gravity drainage reservoir. *Acta Pet. Sin.* **2013**, *34*, 938–946. [[CrossRef](#)]
21. Liang, S.; Zhou, W.; Zhang, J. Investigation on Effect Application of the Technology of Crestal Gas Injection for Stable Gravity Flooding. *J. Southwest Pet. Univ.* **2014**, *36*, 86–92. [[CrossRef](#)]
22. Zhang, Y.; Wang, K.; Li, H.; Li, L.; Nie, F. Study of numerical simulation for gravity drive of crestal nitrogen injection in gas-cap reservoir. *J. China Univ. Pet.* **2006**, *30*, 58–62. [[CrossRef](#)]
23. Ren, S.; Liu, Y.; Zhang, L.; Cui, G.; Gong, Z.; Wang, Y.; Han, B. Gravity assisted gas injection: Assessment model and experimental study. *J. China Univ. Pet.* **2018**, *42*, 59–66. [[CrossRef](#)]